Surface-initiated mechano-ATRP as a convenient tool for tuning of bidisperse magnetorheological suspensions toward extreme kinetic stability[†]

Martin Cvek,(0000-0003-4292-0748)[a,*], Jozef Kollar[b], Miroslav Mrlik,(0000-0001-6203-6795)[a], Milan Masar[a], Pavol Suly[a], Michal Urbanek[a] and Jaroslav Mosnacek,(0000-0001-9160-590X)(L-1387-2019)[b,c,*]

[a]Centre of Polymer Systems, University Institute, Tomas Bata University in Zlín, Trida T. Bati 5678, 760 01 Zlín, Czech Republic

[b]Polymer Institute, Slovak Academy of Sciences, Dubravska cesta 9, 845 41 Bratislava, Slovakia

[c]Centre for Advanced Materials Application, Slovak Academy of Sciences, Dubravska cesta 9, 845 11 Bratislava, Slovakia
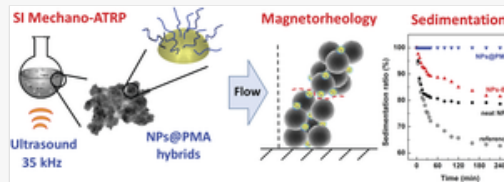
Funding Information

Table of Contents Entry

A concept initially intended for mechanically controlled atom transfer radical polymerization (hereinafter referred to as "mechano-ATRP") was extended in order to modify magnetic nanoparticles (NPs) with poly(methyl acrylate) (PMA) grafts, resulting in NPs@PMA hybrids which served as efficient additives in magnetorheological (MR) suspensions.

Abstract

A concept initially intended for mechanically controlled atom transfer radical polymerization (hereinafter referred to as "mechano-ATRP") was extended in order to modify magnetic nanoparticles (NPs) with poly(methyl acrylate) (PMA) grafts, resulting in NPs@PMA hybrids which served as efficient additives in magnetorheological (MR) suspensions. In a novel procedure, magnetic NPs with an ATRP initiator anchored on their surfaces were added into a mechano-ATRP mixture, bringing about surface-initiated growth of the PMA chains after exposure to ultrasonication (35 kHz, 45 °C). The reaction proceeded with low concentration (at hundreds of "ppm") of the $CuBr_2$ catalyst, thereby providing the PMA chains with low dispersity of molar masses and high monomer conversions. Investigation was conducted as to the effect of hexagonal micro-ZnO and cubic-phase $BaTiO_3$ piezoelectric transducers on the feasibility of the process. The presence of PMA on the surfaces of NPs@PMA hybrids was proven by *infra*-red spectroscopy, as well as thermal and magnetization analyses. The NPs@PMA hybrids were subsequently applied as additives to fabricate a bidisperse MR suspension, in which they unexpectedly enhanced accessible shear stress and yield stress values by up to ~840 Pa under a magnetic field (of up to 432 kA m^{-1}). Notably, the MR suspension supplemented with the NPs@PMA hybrids synthesized by mechano-ATRP exhibited no sign of sedimentation when left undisturbed for 2 days, although sedimentation of the reference sample occurred within a few hours. Such enhancements were attributed to the effects of friction, formation of a 3D gel-like network and the reduced density of the NPs@PMA hybrids.

Introduction

It is anticipated that the global market for smart materials will grow due to augmented use of products that can respond to various stimuli (magnetic/electric fields, mechanical stress, UV-light and alteration in pH or temperature).[1,2] Continuous research is needed to keep up expected demand. This is particularly true for magnetorheological (MR) suspensions, which comprise mixtures of magnetizable micro-particles (1–10 μm) dispersed in a non-magnetic liquid. MR systems exhibit rapid phase transition (in the order of milliseconds) from a liquid-like to solid-like state once a magnetic field is applied.[3] Such a transition, referred to as an "MR effect", is accompanied by exceptional alteration in viscosity and viscoelastic moduli (by several orders of magnitude), which is an important feature in vibration dampers,[4] brakes[5] and clutches,[6] as well as in robotics.[7] When left inactive, a high density mismatch (a 7–8 fold difference) between the particles and carrier liquid causes MR suspensions to exhibit low kinetic stability, exerting a consequent impact on the reliability of the device.[8] Several strategies have been adopted to counteract such gravitational settling; *e.g.* incorporating nanoscale additives[9] and applying various coatings onto the particles[10–12] has proven highly promising.

Nanoparticles (NPs) serve as gap-filling agents that anchor field-induced structures developed from micron-sized analogues. Employing them can enhance yield stress, MR performance and the sedimentation profile.[13,14] An important factor concerns the amount of NPs applied for this purpose, since a "halo" effect occurs beyond a certain threshold (usually at above 5%), weakening the field-induced structures.[14] Various types of NPs, either magnetic or non-magnetic, in different forms, such as spherical,[13] rod-/needle-like[15] and plate-like[16] have been extensively researched.[9] Enhancement of sedimentation stability is best facilitated by NPs with a high surface-to-volume ratio,[17] while magnetic nano-spheres were found to be superior at raising MR performance.[17]

With reference to the latter approach, the benefits of polymer coatings are perceived in decreased bulk density of the resulting core–shell structure and thermo- and chemico-protective effects, which further favour the applicability of the

MR suspensions.[18] Encapsulation techniques involve coupling with low-molecular weight substances, such as organosilanes, or polymers *via* different polymerization methods, *e.g. in situ* dispersion polymerization, suspension polymerization or solvent evaporation.[12] These do not usually give rise to compact polymer layers, however, and the quality of the coating at a molecular level is debatable.

Types of reversible-deactivation radical polymerization (RDRP), such as atom transfer polymerization (ATRP)[18,19] and reversible-addition fragmentation chain transfer (RAFT) polymerization[20] are currently considered the most effective techniques for synthesizing functional and special polymeric/hybrid materials. Whereas the RAFT polymerization has been mostly used for the modification of non-magnetic substrates, such as cellulose,[21] silica NPs, gold nanocrystals or bioNPs,[22] the surface-initiated ATRP has been well established for the modification of magnetic substrates, even for the MR purposes.[23] Unlike free-radical polymerization, RDRP produces polymers with traits that include controlled molar mass, low dispersity of molar mass, defined chain architecture and end functionality; this occurs through the concept of dynamic equilibrium, regulated by a system of redox-based transition metal catalytic system.[24,25] Such dynamic equilibrium is mediated either chemically or externally, the former *via* an activator regenerated by electron transfer (ARGET) ATRP[26] or an initiator for continuous activator regeneration (ICAR) ATRP,[27] whereas the latter occurs *via* physical interventions, such as the application of light irradiation,[28] electric potential[29] or high pressure.[30] With respect to surface engineering, these RDRPs can be initiated from the surface of various substrates allowing manipulation with the hydrophobicity/hydrophilicity,[31] bio-inertness/bioactivity,[32] colloidal stability,[33] adsorption capability[34] *etc*.

Recently, mechanical forces generated by ultrasonic (US) agitation were exploited for precise polymer synthesis, giving rise to a new RDRP technique referred to as mechanically-controlled ATRP (mechano-ATRP).[35] Mechano-ATRP requires the presence of piezoelectric particles that produce an electric charge in response to an applied mechanical stimulus provided by US agitation.[36] The resultant US shock waves induce the electron formation that reduces the deactivator (Cu^{II}) to an activator (Cu^{I}) species, thereby initiating the ATRP process. The concept of mechano-ATRP was introduced recently by Mohapatra *et al.*[35] who synthesized poly(n-butyl acrylate) as a model polymer. They used barium titanate ($BaTiO_3$) NPs as the piezoelectric transducer, since they exhibited sufficient potential to reduce ligand-stabilized (Cu^{II}) complexes. Nevertheless, the process required high catalyst loading (10 000 ppm with respect to the monomer), and relatively low values for molar mass were observed ($M_n < 3000$ g mol^{-1}). Wang *et al.*[25] expanded on the topic by preparing poly(methyl acrylate) (PMA) *via* mechano-ATRP with appreciably low concentration of the catalytic system (75 ppm). The authors also experimented with various $BaTiO_3$ loadings and different crystallography structures, achieving relatively high values for molar mass (M_n of up to 20 000 g mol^{-1}). In their following study[37] they applied zinc oxide (ZnO) NPs as the electron transfer agent instead of those based on $BaTiO_3$. The ZnO NPs showed higher effectiveness, hence significantly lower loadings were sufficient to carry out the polymerization. However, the quantity of polymers synthesized by mechano-ATRP remains rather low, with all of them having been prepared as trial systems in the form of individual polymer chains dispersed in a reaction medium.[25,35–38] Contrary to other RDRPs, the mechano-ATRP has not been ever applied for polymer grafting onto a solid substrate.

This study investigated the immobilization of an ATRP initiator onto magnetic NPs and, for the first time ever, mechano-ATRP was used to grow polymer chains from the surfaces of the NPs, resulting in NPs@PMA hybrids. Taking into consideration the principle of mechano-ATRP, US shock waves were applied to the piezoelectric crystals, thereby initiating simultaneous oxidation and reduction reactions (Cu^{II}/Cu^{I}), which occurred in tandem with a conventional ATRP activation/deactivation cycle.[35] Since ATRP-like conditions existed in the activated state, we presumed that surface-initiated growth of the polymer chains was possible in the vicinity of the piezoelectric nano-transducers. The polymer chains tethered by one chain-end to the substrate of the NPs formed a defined layer capable of improving the characteristics of the MR suspension. Applying a sacrificial initiator enabled optimization of the synthetic route in order to achieve a reasonably high conversion and low dispersity of molar mass, while the impact of two types of piezoelectric transducers – custom-produced micro-ZnO powder and commercial $BaTiO_3$ nanocrystals – was investigated. The next challenge was segregation of the fabricated NPs@PMA hybrids from the mechano-ATRP reaction mixture, which was severely affected by interactions between the product and the piezoelectric transducers.

The success of the grafting process was evaluated subsequently, and the developed NPs@PMA hybrids were studied in relation to their intended application. The polymer chains tethered by one chain-end to the substrate of the NPs formed a defined layer capable of improving the characteristics of the MR suspension. In the final stage, the NPs@PMA comprised the bidisperse MR suspension, the performance of which was determined and compared to the reference, and the mechanisms of the effects of bidispersity thoroughly examined.

Experimental

Materials

All chemicals were sourced from Sigma-Aldrich (USA) if not stated otherwise. The materials utilized to synthesize the micro-ZnO powder comprised zinc acetate dihydrate ($Zn(CH_3COO)_2 \cdot 2H_2O$, ≥98%) and oxalic acid dihydrate ($C_2H_2O_4 \cdot 2H_2O$, ≥99%). The Fe-NPs were based on iron(III) chloride hexahydrate ($FeCl_3 \cdot 6H_2O$) and iron(II) chloride tetrahydrate ($FeCl_2 \cdot 4H_2O$) in an alkaline environment of ammonium hydroxide (NH_4OH). The organosilanes, namely, tetraethoxysilane (TEOS, 98%) and (3-aminopropyl)triethoxysilane (ATPES, ≥98%) were attached to the substrates in ethanol (EtOH, 95%) and isopropanol (≥98%) to ensure their compactness and functionality, respectively. 2-Bromoisobutyryl bromide (BiBB, 98%) was immobilized onto the surface of the NPs in a mixture of tetrahydrofuran (THF, p.a.) and triethylamine (TEA, ≥99%), which were employed as a medium and proton scavenger, respectively. In order to eliminate residual water content, the THF was pre-dried using 4 Å molecular sieves (pellets) and dried over several hours with the aid of fresh sodium wires (≥99%). Methyl acrylate (MA, 99%), ethyl 2-bromoisobutyrate (EBiB, 98%), and tris(2-pyridylmethyl)amine (TPMA, 98%), served as the monomer, sacrificial initiator and ligand, the latter complexing with copper(II) bromide ($CuBr_2$, 99%), respectively. Next, the MA was purified by passing it through a short column of aluminium oxide (basic, Brockmann I) to remove the monomethyl ether hydroquinone inhibitor, while the rest of the chemicals was utilized without treatment. Dimethyl sulfoxide (DMSO, anhydrous, ≥99.9%) was employed as a suitable medium for mechano-ATRP, and nanocrystals of $BaTiO_3$ (≥99%,<100 nm) were used as an electron transfer agent. Aluminium oxide (neutral, Brockman I) served as a depriving agent to remove the catalyst prior to taking GPC measurements. The solvents utilized for the purification of the product, *e.g.* acetone (p.a.) and EtOH, were obtained from Penta Laboratories (Czech Republic). The carbonyl iron (CI) particles (SL grade) supplied by the BASF Corporation (Germany) constituted the primary magnetic filler in the MR suspension. The selected CI grade contains spherical micro-particles of 1–5 μm in a diameter, high purity (above 96 wt% of iron content) and crystallizes in cubic crystalline phase.[13,18] Silicone oil (M15 with the dynamic viscosity of 14.5 mPa s and density of 0.930 g cm^{-3} at 25 °C) was sourced as a commercial product from Lukosiol (Czech Republic) and applied as a suitable carrier liquid.

Synthesis of the micro-ZnO electron transfer transducer

The zinc oxalate dihydrate ($ZnC_2O_4 \cdot 2H_2O$) precursor was prepared by precipitating 500 mL of 0.5 M solution of $Zn(CH_3COO)_2 \cdot 2H_2O$ into 1000 mL of 1 M solution of $C_2H_2O_4 \cdot 2H_2O$. The solution was thoroughly mixed (at 500 rpm) on a magnetic stirrer, and the reaction was performed under laboratory conditions. The precursor was separated by filtration and left to dry at the temperature of 60 °C overnight. It was subsequently annealed at 400 °C for 30 minutes in a muffle furnace. The annealing temperature was reached at a heating rate of 10 °C min^{-1}. Following such exposure to heat, the oven and sample in it were left to cool down without intervention.

Synthesis of magnetic NPs with covalently attached initiator moieties (NPs-Br)

The magnetic NPs were synthesized *via* a simple co-precipitation reaction, in accordance with Song *et al.*[39] In brief, 3.0 g of $FeCl_3 \cdot 6H_2O$ (11.10 mmol) and 2.5 g of $FeCl_2 \cdot 4H_2O$ (12.57 mmol) were dissolved separately in 100 mL of deionized H_2O and degassed with N_2 for 20 minutes to remove the O_2 from the solutions. Both solutions were mixed in a 500 mL round-bottom flask, and 10 mL of NH_4OH were added under vigorous stirring and an N_2 atmosphere. Formation of the NPs was accompanied by a rapid change in colour of the solution, turning from orange to black. The mixture was stirred for an additional 4 hours and a black precipitate (the magnetic NPs) was collected with a magnet. The NPs were washed in several cycles with deionized H_2O and EtOH.

In the next step, 0.3 g of the NPs was dispersed in 150 mL of EtOH concurrently with the addition of 15 mL of deionized H_2O and 12 mL of NH_4OH. The mixture was sonicated for 30 minutes at laboratory temperature and 1.2

mL of TEOS (1.13 g, 5.41 mmol) was added dropwise. The mixture was vigorously stirred for an additional 4 hours to facilitate formation of TEOS layers on the surface of the NPs. These TEOS-coated NPs were collected with a magnet, and any residual TEOS was removed in several washing routines, in the manner described in the previous stage.

The NPs were functionalized afterwards by the APTES. The amount of 0.2 g of the silica-coated NPs was dispersed in 50 mL of isopropyl alcohol, and 0.2 mL of APTES (0.19 g, 0.85 mmol) was added dropwise. The mixture was sonicated for 6 hours at laboratory temperature. The APTES-treated NPs (NPs-NH$_2$) were collected with the magnet and re-dispersed in deionized H$_2$O and EtOH as the washing liquids, while simultaneously removing any free APTES *via* the magnet-assisted decantation method. The NPs-NH$_2$ particles were dried at 50 °C in a vacuum oven.

The initiator was subsequently immobilized through esterification, whereby 0.3 g of NPs-NH$_2$ was transferred into a 50 mL Schlenk flask (SF), which was evacuated and backfilled with argon several times. Next, 20 mL of dried THF and 0.542 mL of TEA (0.39 g, 3.92 mmol) were injected into the flask. The particles were dispersed and the reaction mixture was cooled to 0–5 °C in an ice bath. Finally, 0.242 mL of BiBB (0.45 g, 1.96 mmol) was added dropwise under an argon atmosphere. Based on a theoretical calculation, the BiBB was utilized in excess, *i.e.* 10 BiBB molecules per 1 nm^2 of NPs-NH$_2$, taking into account the specific surface area determined *via* the BET method (Fig. S1 in ESI[†]). The temperature of the ice bath was maintained for 3 hours, and the reaction proceeded overnight under laboratory conditions. The initiator-treated NPs (NPs-Br) were separated by the magnet, washed in the manner stated above and dried at 50 °C in the vacuum oven.
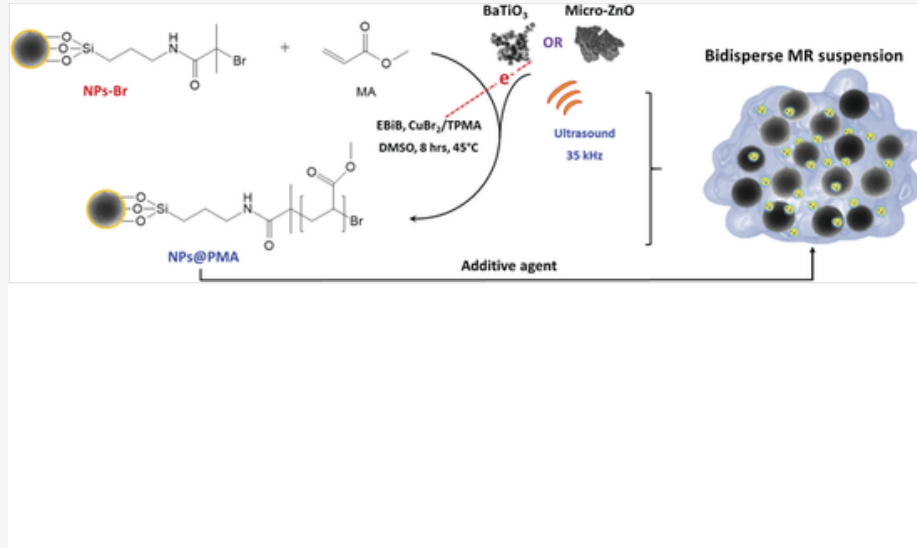
Mechano-ATRP of MA

The general procedure for the mechano-ATRP was inspired by Wang *et al.*[37] with some modifications. Herein, 2 mL of MA (1.91 g, 22 mmol, 200 equiv.), 16.2 μL of EBiB (21.5 mg, 0.11 mmol, 1 equiv.), 5.60 mg of TPMA (19.2 μmol, 0.18 equiv.), 0.72 mg of CuBr$_2$ (3.2 μmol, 0.03 equiv.), 2 mL of DMSO (50 vol%) and either 200 mg of micro-ZnO (5 wt%) or 360 mg of BaTiO$_3$ nanocrystals (9 wt%) were transferred into a 10 mL SF. During the dosing sequence a short course of sonication (1 minute) was applied to accelerate the dissolution of TPMA/CuBr$_2$ and aid dispersion of the piezoelectric transducers. The SF was sealed afterwards and deoxygenation ensued through six freeze–pump–thaw cycles, followed by filling the SF with argon as the last step. The reaction was initiated by immersing the SF into a Sonorex DL 102H ultrasonic (US) bath (Bandelin, Germany) coupled with a temperature controller (Julabo F 12, Germany). The bath operated at a constant temperature of 45 °C, the frequency of 35 kHz and the US power of 300 W (*ca.* 1.4 W cm^{-2}). The reaction was stopped after 8 hours by switching off the US generator and opening the flask to aerate the reaction system.

Surface-initiated mechano-ATRP of PMA

This was performed in a manner similar to the conventional mechano-ATRP analogue. Besides the typical reactants (as above), 50 mg of NPs-Br particles were added as the final component into the reaction mixture, permitting concurrent growth of PMA chains from their surfaces and producing the resultant NPs@PMA hybrids (Fig. 1). The US agitation dispersed the micro-ZnO or BaTiO$_3$ nanocrystals well, in addition to the NPs-Br. The viscosity of the reaction medium increased over time, signifying the growth of the PMA chains. The polymerization process was stopped after 8 hours by switching off the US generator and opening the flask to aerate the reaction system. The binary mixture of the nano-powders was segregated subsequently *via* repetition of the magnet-assisted decantation method and gravitational settling, in accordance with the following procedure. In brief, DMSO was added (12 mL) to decrease the viscosity of the system and facilitate mobility of the NPs@PMA particles toward the magnet, which had been placed on the side of the vial. The non-magnetic BaTiO$_3$ nanocrystals settled down and were removed by decantation. A dose of fresh DMSO was given, the Ns@PMA redispersed and the magnet-assisted decantation process was repeated, this occurring six times. Finally, the NPs@PMA particles obtained were washed several times with ethanol and dried at 50 °C overnight.

Fig. 1

Grafting the NPs-Br with PMA by SI mechano-ATRP, and utilization of the product in bidisperse MR suspension.

Analysis of the polymerization process

Determining the extent of monomer conversion involved carrying out proton nuclear magnetic resonance (^{1}H NMR) spectroscopy in deuterated DMSO (DMSO-d6) on a 400 MHz VNMRS (Varian, UK) spectrometer equipped with a 5 mm 1He19F/15Ne31P PFG AutoX DB NB probe at 25 °C. The chemical shifts were reported in ppm, downfield to the reference signal of TMS. Molar mass and dispersity, Đ, were estimated on a gel permeation chromatography (GPC) instrument (1260 Infinity, Agilent Technologies, USA) equipped with a Waters 515 pump, three PPS SDV-type columns of 8 × 300 mm with 5 μm beads at the porosity of 10^2, 10^3 and 10^5 Å (Polymer Standard Services, Germany) and a Waters 410 differential RI detector. Separation was performed in THF, which served as an eluent at the flow rate of 1.0 ml min^{-1} at 30 °C. The instrument was calibrated with linear PMMA as the standard, while anisole was applied as an internal standard to correct fluctuations in the THF flow rate.

Characterization of the (nano)particles

The morphology and micro-structure of the ZnO transducer was studied by scanning electron microscopy (SEM) on a field-emission SEM device (Nova NanoSEM 450, FEI, Japan) operating at the accelerating voltage of 5 kV. Energy-dispersive X-ray (EDX) spectroscopy was performed on the SEM device after attaching an Octane SSD detector (Ametek). The crystallographic structure of the ZnO was assessed *via* X-Ray diffractions (XRD) on a Miniflex 600 (Rigaku, Japan) diffractometer using a Co-Kα radiation source (λ = 1.789 Å) operating within a 2θ range of 10–95° at the scan speed of 3° min^{-1}.

The presence of a siloxane layer and PMA layers on the surfaces of the NPs was verified by Fourier transform infrared (FTIR) spectroscopy on a Nicolet 6700 (Thermo Scientific, USA) device equipped with an ATR unit and Ge crystal. The dataset was collected in the typical wavenumber region of 4000–700 cm^{-1}, encompassing 64 scans at a resolution of 2 cm^{-1}.

The presence of the grafted PMA layer was also verified by transmission electron microscopy (TEM) on a JEM-2100Plus (JEOL, Japan) instrument equipped with a lanthanum hexaboride LaB6 cathode and set to the accelerating voltage of 200 kV. The sample was prepared by dispersing the NPs in acetone through ultrasonic agitation and dripping them onto a carbon-coated grid (300 mesh, Agar Scientific, UK).

Nitrogen absorption/desorption isotherms (see Fig. S1[†]) were recorded on a volumetric gas adsorption analyzer (BELsorp Mini II, BEL, Japan) at 77 K. Prior to taking measurements the powders were degassed in a sample tube at 60 °C for 5 hours. The specific surface area (SSA) was determined by multipoint Brunauer–Emmett–Teller (BET) analysis, applying at least five data points within a relative pressure range from 0.05 to 0.30.

The isothermal (25 °C) magnetic properties of the particles (*ca.* 5–7 mg in amount) were investigated on a vibrating-sample magnetometer (VSM) (Model 7404, Lake Shore, USA) at the range of ±1150 kA·m^{-1}. VSM spectra were

collected with the amplitude of vibration, frequency of vibration and time constant set to 1.5 mm, 82 Hz and 100 ms, respectively.

Thermal characterization of the particles was performed on a Q500 thermogravimetric analyzer (TGA) (TA Instruments, USA). Each sample (*ca.* 5–10 mg in amount) was subjected to a defined temperature programme across the range of 30–700 °C at a 10 °C min^{-1} heating rate on a platinum pan under a helium atmosphere (50 mL min^{-1}). Prior to analysis the sample chamber (furnace) was purged with helium for 10 minutes to eliminate air content.

Characterizations of MR suspensions

Four MR formulations were fabricated and tested. The reference MR suspension was prepared by dispersing a calculated amount of the CI particles into the silicone oil, thereby yielding a particle concentration of 60 wt%. CI particles were also added into the other three MR suspensions, which were additionally supplemented with 3 wt% of the neat magnetite NPs, NPs-Br or NPs@PMA. MR performance was investigated on an advanced Physica rotational rheometer (MCR 502, Anton Paar, Austria) equipped with a magneto-cell (MRD/170/1 T), set up in parallel-plate configuration (PP20/MRD/Ti) with a gap of 0.3 mm. Shear rates at the range of 10^{-1}–3×10^2 s^{-1} were applied, during which data-points were collected under constant rise in a logarithmic scale. A power source (PS-MRD/5A) served to generate an external magnetic field, applied at the range of 72–432 kA m^{-1} (in increments of 72 kA m^{-1}) in a direction perpendicular to the flow. Characterization was performed at the constant temperature of 25 °C, maintained by a thermostatic device (Julabo FS18, Germany). So as to ensure the same initial conditions, the suspensions were pre-sheared for 60 s at 10^2 s^{-1}. Prior to gauging field-on measurements, the corresponding field was imposed for an additional 60 s to provide sufficient time for inner-structure development. Each suspension was characterized by three independent measurements, for which mean values are presented herein. MR activity was investigated under a dynamic magnetic field to discern the reproducibility of the formation of the internal structure. The MR suspensions were sheared at a constant shear rate of 50 s^{-1} while the magnetic field was periodically (the interval of 30 s) switched on (at 216 kA m^{-1}) and off.

For the sedimentation experiment, the MR suspensions were dosed into Eppendorf tubes, sonicated for 5 minutes and carefully placed in a vertical position in a custom-built holder. The sedimentation ratio, *i.e.* the ratio between the particle-rich phase and the total height of the suspension, was monitored over time on a digital camera (DMK 42BUC03, ImagingSource, Germany) coupled with a manual iris varifocal lens (T3Z3510CS, Computar, Japan). The resulting photographs were analysed in ImageJ software (version 1.52a, National Institute of Health, USA).

Results and discussion

Rationale of the modification technique

The concept of the surface-initiated mechano-ATRP technique was devised to discern its possible advantages over conventional RDRPs, these comprising: (i) low ppm amounts of Cu catalyst as a modern standard in ATRP; (ii) a relatively low reaction temperature; (iii) deep penetration of the US into the heterogeneous system compared to photo-ATRP, for example[40] (iv) great uniformity of radical/activator generation that overcomes the catalyst diffusion limitation of electrochemically-mediated RDRPs, especially at high conversion;[38] and (v) the US not only ensures electron transfer from the piezoelectric transducer to Cu^{II}/L complex, but it also suppresses the gravitational settling of the NPs since magnetic stirring cannot be applied in their presence. Hence, it is possible to realize the grafting process from the entire surface of the NP. Bearing these benefits in mind, the surface-initiated mechano-ATRP technique was designed and tested for the first time. Employing it for surface modification of the NPs was expected to be facilitated by the magnetic properties of the same due to the potential to separate them from the reaction mixture once the mechano-ATRP had finished.

Optimization of conditions for mechano-ATRP

The appropriate level of piezoelectricity is critical to successfully conducting the mechano-ATRP. Piezoelectricity can be driven through the crystallographic structure of the mechano-transducers, their size and surface-to-volume ratios.[25] ZnO is relatively efficient at polymerizing acrylate monomers by mechano-ATRP and requires much lower loading than BaTiO$_3$.[37] Custom-produced hexagonal micro-ZnO was selected as the potential candidate for establishing the

reaction conditions. The morphology, elemental analysis and XRD patterns of the custom-produced micro-ZnO powder are discussed in the ESI (Fig. S2).[†] Using 5 wt% of micro-ZnO, in the polymerization of MA (at a temperature below 45 °C, 35 kHz) brought about a monomer conversion of 75% after 8 hours, giving rise to PMA with $M_n = 14$ 000 g mol^{-1} and $Đ = 1.26$ (Fig. S3[†]).

Commercial cubic-phase BaTiO$_3$ nanocrystals were employed in parallel as the mechano-electric transducer. In order to accelerate the polymerization rate of the typically less efficient BaTiO$_3$ (mg mg^{-1}), the loading of 9 wt% was found to be needed for successful and reasonably rapid polymerization. With this loading the mechano-ATRP (at a temperature below 45 °C, 35 kHz) led to the monomer conversion of 74% after 8 hours, resulting in PMA with $M_n =$ 13 300 g mol^{-1} and $Đ = 1.09$ (Fig. S3[†]). Slightly slower polymerization was reported by Wang et al.[25] for tetragonal-phase BaTiO$_3$ NPs (200 nm) at the same loading (other conditions remained constant). Although tetragonal BaTiO$_3$ has a larger dielectric constant than its cubic-phase analogue,[41] it is believed that the effective surface area plays a crucial role in the efficacy of the electron transfer process. Even though the SSA value of the tetragonal BaTiO$_3$ was not stated by said authors,[25] a lower value for SSA of their particles is likely considering the larger particle diameter reported in comparison to the cubic-phase BaTiO$_3$ reported herein.

So as to obtain better insight into the interfacial effects, the solid-state reactants were characterized by N$_2$ physisorption (Fig. 2a). The custom-produced hexagonal micro-ZnO exhibited a total pore volume of 0.235 cm^3 g^{-1}, while the SSA value equalled 30 m^2 g^{-1}. The commercial BaTiO$_3$ was characterized as having a total pore volume of 0.148 cm^3 g^{-1} and SSA value of 17 m^2 g^{-1}, as determined by BET. It would appear that the value for SSA is highly relevant to mechano-ATRP as it affects the ability of the particles to reduce the deactivator, thus it influences the extent to which radicals are generated. For this reason, a lesser amount (5 wt%) of the micro-ZnO sufficed to achieve a conversion comparable to 9 wt% of the BaTiO$_3$.

Fig. 2
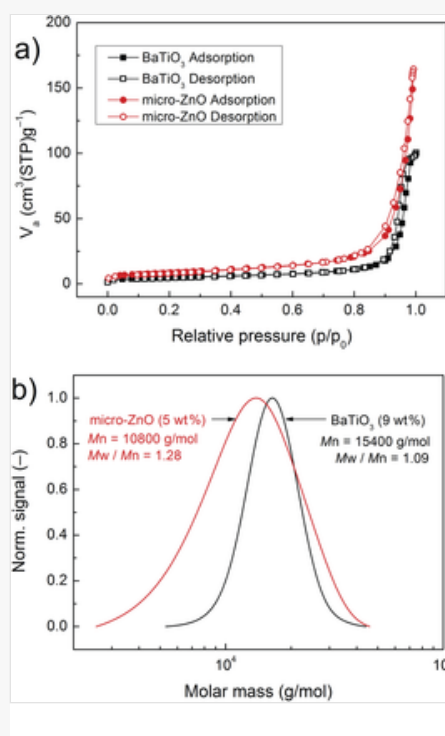
Nitrogen adsorption/desorption isotherms (a) for the BaTiO$_3$ nanocrystals (black) and micro-ZnO (red), and GPC traces (b) of PMA synthesized from the sacrificial initiator during surface-initiated mechano-ATRP mediated by cubic-phase BaTiO$_3$ and hexagonal micro-ZnO.

Synthesis of magnetic NPs@PMA hybrids by mechano-ATRP

This section describes the first time that surface-initiated mechano-ATRP has been employed to fabricate NPs@PMA hybrids. The novel method complements existing techniques and is capable of synthesizing well-defined polymer chains. Besides the typical reactants (as above), NPs-Br particles at the amount of 50 mg were introduced into the

reaction mixture as a suitable substrate. In terms of surface properties, the NPs-Br exhibited the SSA from which the polymer chains could grow value of 36 m^2 g^{-1}. Applying hexagonal micro-ZnO as the electron transfer agent led to 62% monomer conversion after 8 hours, providing PMA with M_n = 10 800 g mol^{-1} and Đ = 1.28. In the system mediated with cubic-phase BaTiO$_3$, conversion reached 80% after 8 hours and a polymer with M_n = 15 400 g mol^{-1} and Đ = 1.09 was obtained (Fig. 2b). The very low values for Đ in this case implied that a high level of control was exerted over the polymerization. The GPC characteristics were obtained from solution phase containing the free (unattached) PMA chains as the side product. The evaluation was made assuming that M_n and Đ of the grafted PMA and those of the free PMA are similar, which is a frequently used method.[42,43]

A cleaning protocol to segregate the binary reaction mixture was additionally developed. By carrying out cyclic magnet-accelerated decantation and gravitational settling, it was possible to separate the BaTiO$_3$ nanocrystals and NPs@PMA hybrids from the reaction mixture (Fig. 3). Nevertheless, this was not sufficient to segregate the micro-ZnO and the NPs@PMA hybrids, a phenomenon explained by the forces of attraction between these two agents and the complex structure of the ZnO that entrapped the magnetic NPs upon exposure to the US shock waves. Hence, further investigation focused solely on the NPs@PMA hybrids fabricated *via* surface-initiated mechano-ATRP when employing BaTiO$_3$ nanocrystals as the electron transfer agent.

Fig. 3
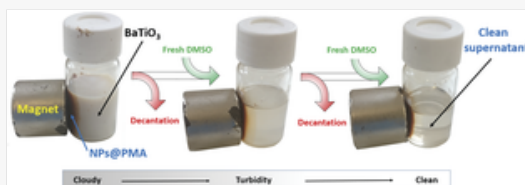
Process for segregation of the NPs@PMA from the BaTiO$_3$ reaction mixture; in total, 6 cycles of ultrasonication, segregation and decantation were performed.

Characterization of the NPs@PMA

The NPs@PMA particles were analysed by various instrumental methods in order to confirm the grafting process and investigate the magnetic properties of the particles. FTIR spectroscopy was carried out to discern the structure of the magnetic NPs at various stages of the synthesis procedure. Fig. 4 displays the FTIR spectra for the neat NPs, NPs-Br and NPs@PMA. The spectrum for the neat NPs exhibits a broad absorption band at about 3400 cm^{-1}, which is typical for vibrations of absorbed H$_2$O and surface OH groups.[44,45] Peaks related to Fe–OH bending and Fe–O stretching mode are usually detected[45,46] at around 685 cm^{-1} and 586 cm^{-1}, respectively, which exceed the investigated limit of 700 cm^{-1}. Apart from these signals, iron oxide does not normally exhibit any characteristic bands.[44] In contrast, the spectrum for the NPs-Br particles shows a dominating peak at 1071 cm^{-1} that can be attributed to Si–O–Si asymmetric stretching, this being typical for organosilanes.[23] Raised absorption levels at 951 cm^{-1} and 804 cm^{-1} also indicated Si–O and Si–C stretching vibrations, respectively. Following the PMA grafting experiment, a series of peaks appeared. In this context the signature peak at 1738 cm^{-1} is a clear sign of C=O stretching of the ester group, while the one at 2958 cm^{-1} indicates C–H stretching.[47] The strong Si–O–Si peak exhibits a red shift to 1076 cm^{-1}. The energy absorbed at 1261 cm^{-1} and 1160 cm^{-1} is assigned to C–O–C stretching in the ester groups of the PMA. The sharp peak at 1437 cm^{-1} is a characteristic sign of the antisymmetric deformation of the CH$_3$ pendant group. As a consequence it can be claimed that FTIR analysis convincingly proved the presence of the PMA layer grafted onto the substrate by the method of surface-initiated mechano-ATRP.

Fig. 4
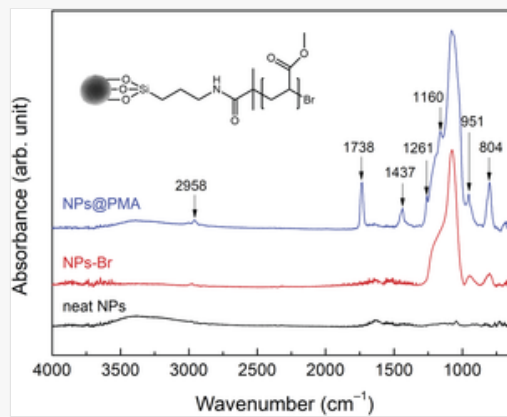
FTIR spectra for the neat NPs, NPs-Br and NPs@PMA with highlighted characteristic peaks.

The presence of the grafted layers was further confirmed by TEM; Fig. 5 shows TEM micrographs for the investigated samples. The neat NPs were almost spherical with smooth surfaces and of 11.8 ± 2.7 nm in dimension. The primary particles formed bigger aggregates despite the applied sonication.[39] It is likely that the aggregation on the TEM grid occurred due to drying phenomenon, upon which the capillary forces can overcome the repulsive forces brining the NPs together.[48] The NPs-Br developed similarly complex structures, however, a thin layer on their surface was detected and attributed to TEOS and BiBB agents. Besides, the aggregation of these species could be a consequence of inter-particulate Si−O−Si bonding that takes place during silanization. The NPs@PMA possessed a relatively thick (~15 nm) low-contrast shell, this confirming that PMA had been grafted. In this case, the aggregation was related also to tangling effects of the polymer chains.[48] Although it seems that the final additive took the form of multiple magnetic cores encapsulated with the PMA shell, it was observed that the NPs@PMA aggregation was reversible, and the NPs@PMA aggregates reconstituted into smaller entities in oil-based environment once exposed to an ultrasound. This could explain their extreme stabilization effects when introduced into bidisperse MR suspensions (shown below). Sparsely distributed $BaTiO_3$ nanocrystals were additionally found in the sample, entrapped in the aggregates during the polymerization process.
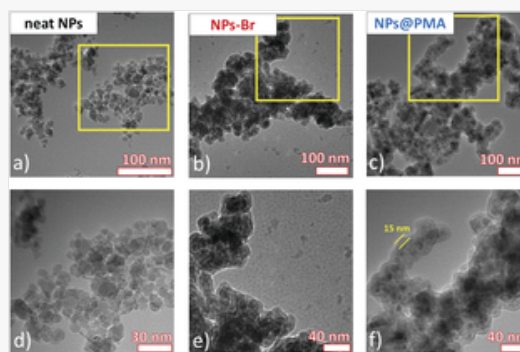

Representative TEM images of the neat NPs (a), NPs-Br (b) and NPs@PMA (c); the corresponding regions of interest are magnified (d, e and f).

TGA was carried out to determine the amount of grafted material on the NPs, and the corresponding curves are displayed in Fig. 6. The Neat NPs showed steady decrease in weight, resulting in a total weight loss of 4.5 wt%, which stemmed from the removal of physically adsorbed water and cleavage of H_2O molecules from the surface of the NPs.[49] The intermediate products – $NPs-NH_2$ and NPs-Br – exhibited similar trends, albeit with greater weight loss of 7.7 wt%, and 9.5 wt%, respectively. The data indicated the presence of TEOS/APTES and that the BiBB initiator had successfully attached to the NPs. Finally, the NPs@PMA exhibited a two-stage degradation process. The first stage (below 100 °C) is attributable either to water evaporation or residual amounts of the washing liquids or traces of the monomer. The latter stage of weight loss (point of inflexion at 406 °C) was a consequence of PMA decomposition, similar to that observed by Arsalani et $al.$[49] on poly(vinyl pyrrolidone)-coated Fe_3O_4 NPs. Total loss of mass in the

temperature range of 300–500 °C, assigned to the decomposition of the PMA layer on NPs@PMA, equalled 11 wt%, corresponding to the grafting density of approximately 0.2 PMA chains per nm^2 of the NPs.


Fig. 6
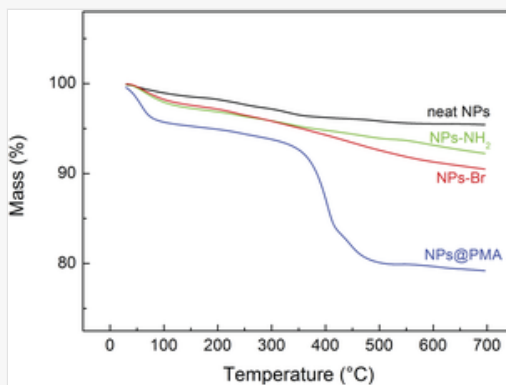
TGA curves for the neat NPs, NPs-NH$_2$, NPs-Br and NPs@PMA under a helium atmosphere.

The effect of the non-magnetic layers after each step of modification on the magnetic properties of the NPs was investigated by VSM. Fig. 7 compares the magnetization curves of the magnetic powders that were utilized to constitute the bidisperse MR suspension. The highest saturation magnetization (M_S), close to 214 emu per g, was observed for the neat CI particles. The original NPs were characterized by an M_S of ~65.7 emu per g, which is a typical value for iron oxides prepared by co-precipitation.[49] This indicates that some cation sites were occupied by Fe^{2+} since the M_S value for pure Fe$_3$O$_4$ is close to 92 emu per g.[45] After encapsulation with the silica layer, the M_S decreased to ~35.6 emu per g, while an additional decrease of 8.7 emu per g was observed after immobilization of the BiBB. The NPs@PMA exhibited the lowest magnetization, with a value for M_S of ~10.8 emu per g. According to the literature,[16] additives demonstrating M_S even in the order of units [emu per g] are still suitable for MR-related application. As detailed later, the magnetization of additives is not the only factor that affects the rheological performance of MR suspensions. Note that all the magnetic fillers utilized possessed negligible remanence and coercivity (Fig. 7, inset), suggesting rapid magnetization/demagnetization cycles in potential MR devices.
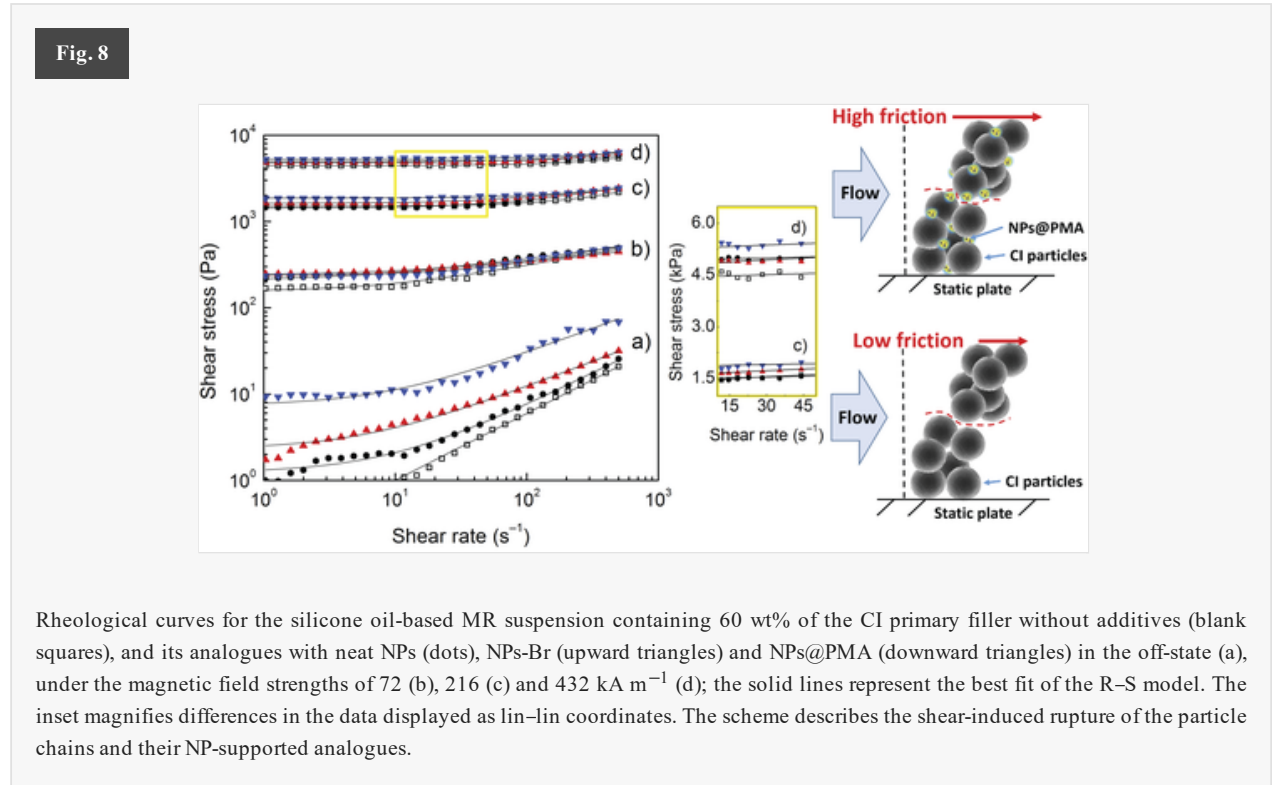

Fig. 7
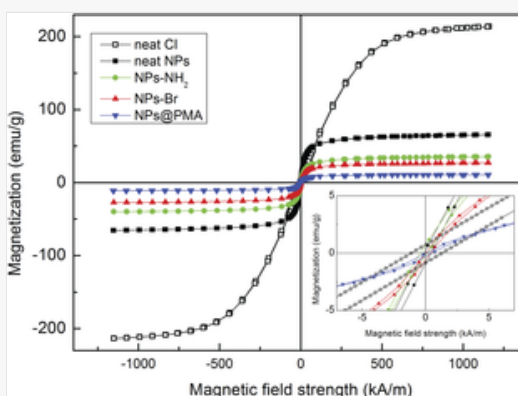
Isothermal VSM curves for the CI particles, neat NPs, NPs-NH2, NPs-Br and NPs@PMA.

Field-responsive properties and the stability of the bidisperse MR suspensions

It is worth mentioning that the concentration applied of the additives was a value informed by the complex behaviour of the MR suspensions. The presence of additives primarily manifests itself in the off-state behaviour and sedimentation stability of bidisperse MR suspensions.[9] Taking into consideration data from a preceding study,[17] applying the additives at an amount of 1 wt% brought about negligible improvement in sedimentation stability, while the amount of

5 wt% inevitably increased off-state viscosity. To balance out these competing effects, the performance of bidisperse MR suspensions was investigated with 3 wt% of the additives, a quantity within the typical range of additive loading.[50]

The rheological properties of the additive-loaded MR suspensions were investigated and compared to the reference, *i.e.* the MR suspension without any additive. Besides the impact of the final NPs@PMA, the trends of flow properties were monitored when the nano-species were applied at various stages of the coating process, as shown in Fig. 8. Emphasis was initially placed on addressing changes observed under off-state conditions. The reference suspension exhibited the lowest off-state shear stress, which progressively increased after introducing the NPs and their coated analogues (although the concentration, w/w%, of the additives was kept constant). The upward shift in the flow curves occurred due to increased viscous dissipation that usually transpires through increase in the concentration of an additive.[17,51] Such a rise evident herein most likely stemmed from the greater hydrodynamic volume of the supplemented additives lent by the lightweight coatings. Furthermore, enhanced interaction with the silicone oil played a significant role in heightening the rheological response, as discussed below.

Fig. 8

Rheological curves for the silicone oil-based MR suspension containing 60 wt% of the CI primary filler without additives (blank squares), and its analogues with neat NPs (dots), NPs-Br (upward triangles) and NPs@PMA (downward triangles) in the off-state (a), under the magnetic field strengths of 72 (b), 216 (c) and 432 kA m^{-1} (d); the solid lines represent the best fit of the R–S model. The inset magnifies differences in the data displayed as lin–lin coordinates. The scheme describes the shear-induced rupture of the particle chains and their NP-supported analogues.

In order to analyse the differences in the flow curves in detail, the Robertson–Stiff (R–S) model,[52] given by the following equation (eqn (1)), was used:

$$\tau = \left[K^{\frac{1}{n}} |\dot{\gamma}|^{\frac{n-1}{n}} + \left(\frac{\tau_0}{|\dot{\gamma}|} \right)^{\frac{1}{n}} \right]^n \dot{\gamma}$$

(1)

In this model, τ is shear stress, τ_0 is dynamic yield stress and $\dot{\gamma}$ denotes the shear rate, while K and n are the consistency index and power-law exponent, respectively. The R–S model was applied to fit the data at shear rates of $\dot{\gamma}$ > 1 s^{-1}, exhibiting a reasonable correlation (R^2 > 0.94 in the majority of cases) with on-state data and satisfactorily fitting off-state data. It is notable that the additive-loaded MR suspensions exhibited limited, yet measurable, yield stress even in the off-state; the suspension supplemented with NPs@PMA demonstrated a τ_0 of ~10 Pa. A hypothesis is that grafting the PMA increased the number of contacts, thereby forming gel-like networks in the suspension and increasing the viscosity of the mixture. Similar behaviour was observed in the MR suspensions after incorporating high surface-to-volume ratio additives, such as carbon nanotubes[17] or sepiolite clay.[51] The formation of a gel-like structure was also evidenced through a gradual drop in the *n*-index value, reflecting its non-Newtonian properties. The off-state *n*-index

extracted from the R–S equation equalled 0.78 for the reference MR suspension, decreasing to 0.76, 0.59 and 0.51 after incorporating the neat NPs, NPs-Br and NPs@PMA, respectively.

The activity of the MR suspensions in a magnetic field was also investigated. A typical aspect was that τ increased by several orders of magnitude (*e.g.* 1000 times under 432 kA m^{-1}) in the on-state, caused by field-induced formation of robust particle chains with high hydrodynamic resistance that spanned the geometry.[53,54] The scheme in Fig. 8 details the action of the prepared nano-additives in the MR suspension during a shear test. In general, the NPs served as gap fillers, occupying spaces between micro-CI particles. Modifying the NPs by mechano-ATRP resulted in the highest τ values of all the samples in the corresponding fields, due to strong energy dissipation during rupture of the particle chains. The flow curves revealed that the NPs-Br provided enhancement effects comparable to the NPs@PMA in a low magnetic field (72 kA m^{-1}). However, a stronger such effect of the NPs@PMA was detected when exposed to greater magnetic fields. This could be explained by the expulsion of the neat NPs and NPs-Br additives from the field-induced structures of the CI particles.[51] Expulsion of the NPs@PMA has the potential to be less favourable energetically than the related analogues due to the friction effects of the PMA. Thus, they can remain entrapped in the oriented structures in high magnetic fields, further increasing magnetic susceptibility. Such behaviour demonstrates the significance of PMA grafting in enhancing MR performance.

Special attention was paid to τ_0, which probably represents the most relevant rheological value since it describes the performance of the MR suspensions. Fig. 9a shows values for τ_0 plotted as a function of magnetic field strength, H, as applied to the suspensions. According to the theoretical magnetic-polarization model,[10] τ_0 scales as $\propto H^2$ under a weak magnetic field, and after exceeding localized saturationmagnetization, τ_0 follows the same power-law trend as $\propto H^{3/2}$. This behaviour was distinguishable in the MR suspension without the additives, and the exponents equalled 2.05 under weak magnetic fields and 1.58 after exceeding localized saturation magnetization, respectively. Once the magnetic NPs had been incorporated, higher τ_0 values were obtained, reflected in a lower slope (in the range of 1.73 to 1.87) in the first region; manifest as a consequence of the NPs that magnetically saturated (Fig. 7) in low magnetic fields.[55] The other aspect of dependence adhered to the standard magnetic-polarization model in all cases, with the exponent ranging from 1.53 to 1.58. Taking into consideration the extent of magnetization facilitated, adding the NPs@PMA increased values for dynamic τ_0 throughout the entire range of H. Major relative enhancement was detected under low magnetic fields, evidenced by an increment in τ_0 by 46% under 72 kA m^{-1} in comparison with the reference. In terms of absolute τ values, the MR suspension supplemented with the NPs@PMA produced greater τ_0 than the reference to the extent of ~840 Pa (*i.e.* a rise of 18% under 432 kA m^{-1}). Since the magnetization of the NPs@PMA was considered low (Fig. 7), it was proposed that the dominating mechanism of such enhancement in τ_0 stemmed from friction effects and non-polar interactions between the PMA grafts and silicone oil.


Fig. 9
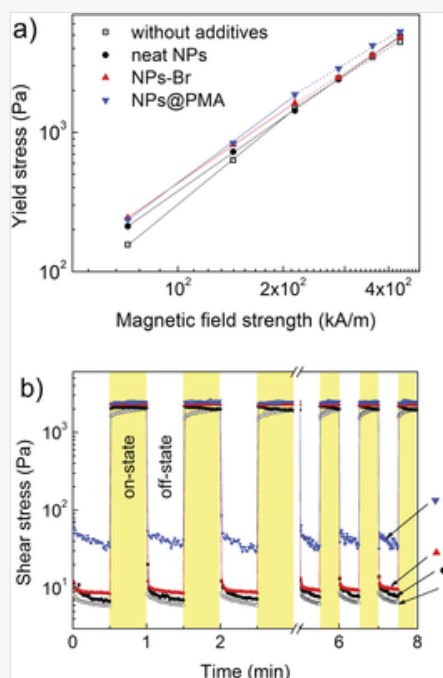
Dynamic yield stress as a function of the magnetic field strength applied (a), reversibility of the structure formation through switching on/off the magnetic field (b) for the silicone oil-based MR suspension containing 60 wt% of the CI primary filler without additives (open symbols), and its analogues supplemented with neat NPs (black circles), NPs-Br (red upward triangles) and NPs@PMA (blue downward triangles).

The samples were additionally subjected to constant shear testing in the presence of an intermittent magnetic field. The variation in τ over time for the inspected MR suspensions is shown in Fig. 9b. It is clear that the magnetic field induced in τ something of a periodic aspect. In the case of the reference MR suspension, the on-state data exhibited a time-dependent characteristic until a steady state was achieved. Somewhat different behaviour was observed in the bidisperse MR analogues, these requiring a shorter time to achieve an on-state plateau. This quality was caused by both the induced magnetization and rapidity of the particle build-up process, which could be of benefit in actual MR devices.[56] Repeatability was verified after several loading cycles, indicating that irreversible friction-induced degradation of the particles had not occurred. In summary, adding the magnetic NPs enhanced the field-sensitivity of the MR suspensions, the sample containing the NPs@PMA exhibiting the highest τ_0 values across the entire range of H, thereby indicating the potential it has for real-world application.

Stability against gravitational settling was assessed through observation with the naked eye of the macroscopic phase boundary between the supernatant oil and particle-rich portion of the MR suspension. Fig. 10 details the sedimentation ratio as a function of time for the given samples. The presence of different nano-species evidently had a remarkable effect on the sedimentation behaviour of the bidisperse MR suspensions. The reference suspension exhibited rapid velocity in sedimentation due to variance in high density between its components, in accordance with Stokes's law.[57] This suspension achieved a state of equilibrium even faster than in a prior study,[17] as a consequence of applying the low viscosity oil (see the section Materials). Adding the neat NPs slightly improved the sedimentation profile through steric hindrance, which prevented large CI particles from aggregating, caused by a mismatch in reduced density between the dispersed nano-/particles and silicone oil.[58] The same content (w/w%) of the NPs-Br resulted in better sedimentation stability in spite of their lower SSA value (36 m^2 g^{-1}) compared to the neat NPs (110 m^2 g^{-1}). It would appear that the dominating mechanism of such additional enhancement arose through application of the low-density TEOS/APTES coatings. Most importantly, the MR suspension containing the NPs@PMA exhibited little-to-no sign of gravitational settling when left undisturbed for 2 days. Such a remarkable difference in sedimentation behaviour likely came about through several factors, including increased hydrodynamic volume, reduced density, the wetting effect and stretching of the PMA molecular chains into the carrier liquid, which enhanced the thixotropy of the bidisperse MR suspension.[59] Moreover, grafting density (of 0.2 PMA chains per nm^2) was considered as sufficient to provide the PMA chains partially extended away from the surface of the NPs, in this way forming the "polymer brush" rather than mushroom conformation.[31] As a result, the PMA chains efficiently decreased the nearest-neighbour inter-particle distances,[33] improving the steric interaction and stability of the MR suspension. The thickening effect of the NPs@PMA, whereby the exceptional sedimentation stability was ensured, correlated with the increase in the τ_0 that could be considered tolerable. The bidisperse MR suspension containing the NPs@PMA also exhibited the most sizeable cake formation in sedimentation, suggesting its easy redispersibility and indicating the superior, long-term readiness of the MR system for actual application. A time-lapse video of the sedimentation test is appended as supporting material in electronic form.

Fig. 10
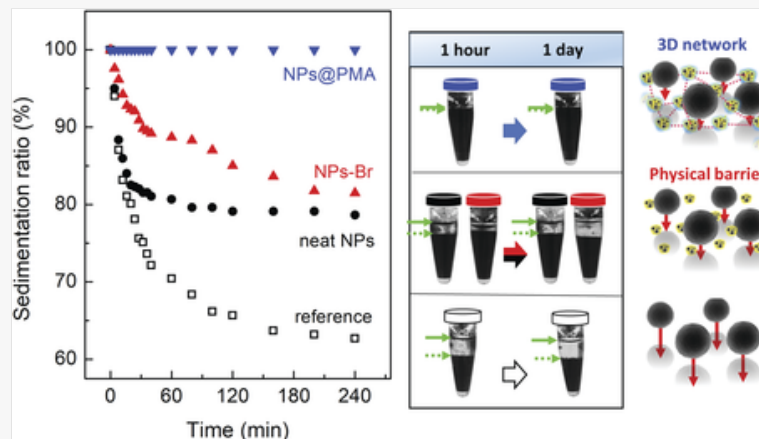
Sedimentation ratio of the silicone oil-based reference MR suspension containing 60 wt% of the CI primary filler (blank squares), and its bidisperse analogues containing the neat NPs (circles), NPs-Br (upward triangles) and NPs@PMA (downward triangles). The scheme demonstrates the mechanism of gravitational settling; while the neat NPs and NPs-Br served as a physical barrier, the presence of the NPs@PMA resulted in formation of a three-dimensional, gel-like network that impeded gravitational settling.

Conclusions

The concept of surface-initiated mechano-ATRP was introduced as a means of synthesizing magnetic NPs@PMA hybrids applicable in magnetorheology. Custom-produced hexagonal micro-ZnO and cubic-phase BaTiO$_3$ nanocrystals were tested as piezoelectric transducers with the aim of facilitating polymerization. Although the BaTiO$_3$ nanocrystals were less efficient (mg mg^{-1}) than the micro-ZnO ones, the former were selected since they permitted extraction of the product from the reaction mixture by sequential cycles of ultrasonication, segregation and decantation. The reaction proceeded in the selected system under mild conditions (45 °C, 35 kHz), exhibiting a high level of conversion of 80% after 8 hours. In addition, polymerization control was seen to be excellent, providing PMA with M_n = 15 400 g mol^{-1} and $Đ$ = 1.09. The presence of grafted PMA was confirmed by FTIR analysis, although the PMA grafts of ~15 nm thickness were also distinguishable from TEM micrographs. The VSM showed gradual decrease in values for M_S, starting at ~65.7 emu per g for the neat NPs and decreasing to ~10.8 emu per g for the NPs@PMA. Despite having a lower value for M_S, the MR suspension supplemented with the NPs@PMA exhibited the best MR performance, with substantially higher values for absolute τ and dynamic τ_0 than its bidisperse analogues with the same content of neat NPs and NPs-Br. Several factors were identified as the cause of such behaviour, including greater hydrodynamic volume, increased friction and susceptibility after bidispersion with the NPs@PMA. This additive also enhanced the sensitivity of the MR suspension in dynamic magnetic fields. The importance of the PMA layer obtained *via* the mechano-ATRP became apparent in the sedimentation test, as the NPs@PMA developed a 3D network structure which prevented the CI particles from undergoing gravitational settling; indeed, almost no sedimentation occurred within the investigated time of 2 days. This represented a dramatic enhancement over the reference sample, which settled after just 3 hours. Thus, surface-initiated mechano-ATRP was proven to be a convenient method for producing polymer/hybrid nano-objects that could serve as efficient additives in MR suspensions.

Conflicts of interest

There are no conflicts to declare.

Acknowledgements

1 L. Y. Tan, A. C. Davis and D. J. Cappelleri, *Adv. Funct. Mater.*, 2020, **56**, 2007125.

2 M. L. Wei, Y. F. Gao;, X. Li and M. J. Serpe, *Polym. Chem.*, 2017, **8**, 127–143.

3 J. de Vicente, D. J. Klingenberg and R. Hidalgo-Alvarez, *Soft Matter*, 2011, **7**, 3701–3710.

4 J. Roupec, F. Jenis, Z. Strecker, M. Kubik and O. Machacek, *Materials*, 2020, **13**, 4670.

5 H. Shamieh and R. Sedaghati, *Smart Mater. Struct.*, 2017, **26**, 125012.

6 A. G. Olabi and A. Grunwald, *Mater. Des.*, 2007, **28**, 2658–2664.

7 J. S. Oh and S. B. Choi, *J. King Saud Univ., Sci.*, 2017, **29**, 390–400.

8 K. Shahrivar and J. de Vicente, *Smart Mater. Struct.*, 2014, **23**, 025012.

9 M. Ashtiani, S. H. Hashemabadi and A. Ghaffari, *J. Magn. Magn. Mater.*, 2015, **374**, 716–730.

10 F. F. Fang, H. J. Choi and Y. Seo, *ACS Appl. Mater. Interfaces*, 2010, **2**, 54–60.

11 F. F. Fang, Y. D. Liu, H. J. Choi and Y. Seo, *ACS Appl. Mater. Interfaces*, 2011, **3**, 3487–3495.

12 B. J. Park, F. F. Fang and H. J. Choi, *Soft Matter*, 2010, **6**, 5246–5253.

13 M. Cvek, R. Torres-Mendieta, O. Havelka, M. Urbanek, T. Plachy and M. Cernik, *J. Cleaner Prod.*, 2020, **254**, 120182.

14 G. R. Iglesias, M. T. Lopez-Lopez, J. D. G. Duran, F. Gonzalez-Caballero and A. V. Delgado, *J. Colloid Interface Sci.*, 2012, **377**, 153–159.

15 T. Plachy, M. Cvek, Z. Kozakova, M. Sedlacik and R. Moucka, *Smart Mater. Struct.*, 2017, **26**, 025026.

16 M. Machovsky, M. Mrlik, T. Plachy, I. Kuritka, V. Pavlinek, Z. Kozakova and T. Kitano, *RSC Adv.*, 2015, **5**, 19213–19219.

17 M. Cvek, M. Mrlik, R. Moucka and M. Sedlacik, *Colloids Surf., A*, 2018, **543**, 83–92.

18 M. Cvek, M. Mrlik, M. Ilcikova, T. Plachy, M. Sedlacik, J. Mosnacek and V. Pavlinek, *J. Mater. Chem. C*, 2015, **3**, 4646–4656.

19 B. Hu, A. Fuchs, S. Huseyin, F. Gordaninejad and C. Evrensel, *Polymer*, 2006, **47**, 7653–7663.

20 J. Sutrisno, A. Fuchs, H. Sahin and F. Gordaninejad, *J. Appl. Polym. Sci.*, 2013, **128**, 470–480.

21 J. Yuan, X. B. Huang, P. F. Li, L. Li and J. Shen, *Polym. Chem.*, 2013, **4**, 5074–5085.

22 L. Wu, U. Glebe and A. Boker, *Polym. Chem.*, 2015, **6**, 5143–5184.

23 M. Cvek, M. Mrlik, M. Ilcikova, J. Mosnacek, L. Munster and V. Pavlinek, *Macromolecules*, 2017, **50**, 2189–2200.

24 K. Matyjaszewski, *Macromolecules*, 2012, **45**, 4015–4039.

25 Z. H. Wang, X. C. Pan, J. J. Yan, S. Dadashi-Silab, G. J. Xie, J. N. Zhang, Z. H. Wang, H. S. Xia and K. Matyjaszewski, *ACS Macro Lett.*, 2017, **6**, 546–549.

26 A. Simakova, S. E. Averick, D. Konkolewicz and K. Matyjaszewski, *Macromolecules*, 2012, **45**, 6371–6379.

27 D. Konkolewicz, A. J. D. Magenau, S. E. Averick, A. Simakova, H. K. He and K. Matyjaszewski, *Macromolecules*, 2012, **45**, 4461–4468.

28 D. Bondarev, K. Borska, M. Soral, D. Moravcikova and J. Mosnacek, *Polymer*, 2019, **161**, 122–127.

29 A. J. D. Magenau, N. C. Strandwitz, A. Gennaro and K. Matyjaszewski, *Science*, 2011, **332**, 81–84.

30 P. Kwiatkowski, J. Jurczak, J. Pietrasik, W. Jakubowski, L. Mueller and K. Matyjaszewski, *Macromolecules*, 2008, **41**, 1067–1069.

31 Y. Tsujii, K. Ohno, S. Yamamoto, A. Goto and T. Fukuda, *Adv. Polym. Sci.*, 2006, 1–45, DOI: 10.1007/12_063.

32 C. F. Huang, *Polym. J.*, 2016, **48**, 341–350.

33 K. Ohno, T. Morinaga, S. Takeno, Y. Tsujii and T. Fukuda, *Macromolecules*, 2006, **39**, 1245–1249.

34 C. F. Huang, J. K. Chen, T. Y. Tsai, Y. A. Hsieh and K. Y. A. Lin, *Polymer*, 2015, **72**, 395–405.

35 H. Mohapatra, M. Kleiman and A. P. Esser-Kahn, *Nat. Chem.*, 2017, **9**, 135–139.

36 I. Zaborniak and P. Chmielarz, *Materials*, 2019, **12**, 3600.

37 Z. H. Wang, X. C. Pan, L. C. Li, M. Fantin, J. J. Yan, Z. Y. Wang, Z. H. Wang, H. S. Xia and K. Matyjaszewski, *Macromolecules*, 2017, **50**, 7940–7948.

38 C. Bian, Y. N. Zhou and Z. H. Luo, *AIChE J.*, 2020, **66**, e16746.

39 W. X. Song, M. Muthana, J. Mukherjee, R. J. Falconer, C. A. Biggs and X. B. Zhao, *ACS Biomater. Sci. Eng.*, 2017, **3**, 1027–1038.

40 G. Zain, D. Bondarev, J. Dohanosova and J. Mosnacek, *Chemphotochem*, 2019, **3**, 1138–1145.

41 V. Petrovsky, T. Petrovsky, S. Kamlapurkar and F. Dogan, *J. Am. Ceram. Soc.*, 2008, **91**, 1814–1816.

42 S. H. Lee, D. R. Dreyer, J. H. An, A. Velamakanni, R. D. Piner, S. Park, Y. W. Zhu, S. O. Kim, C. W. Bielawski and R. S. Ruoff, *Macromol. Rapid Commun.*, 2010, **31**, 281–288.

43 D. R. Wang, G. Ye, X. L. Wang and X. G. Wang, *Adv. Mater.*, 2011, **23**, 1122–1125.

44 P. Peer, M. Cvek, M. Urbanek and M. Sedlacik, *J. Appl. Polym. Sci.*, 2020, **137**, e49576.

45 S. F. Zhang, W. Wu, X. H. Xiao, J. Zhou, F. Ren and C. Z. Jiang, *Nanoscale Res. Lett.*, 2011, **6**, 89.

46 G. H. Qiu, Q. Wang, C. Wang, W. Lau and Y. L. Guo, *Ultrason. Sonochem.*, 2007, **14**, 55–61.

47 A. K. Kushwaha, N. Gupta and M. C. Chattopadhyaya, *Arabian J. Chem.*, 2017, **10**, S1645–S1653.

48 S. Shrestha, B. Wang and P. Dutta, *Adv. Colloid Interface Sci.*, 2020, **279**, 102162.

49 N. Arsalani, H. Fattahi and M. Nazarpoor, *eXPRESS Polym. Lett.*, 2010, **4**, 329–338.

50 M. Nejatpour, U. Unal and H. Y. Acar, *J. Ind. Eng. Chem.*, 2020, **91**, 110–120.

51 J. A. Marins, T. Plachy and P. Kuzhir, *J. Rheol.*, 2019, **63**, 125–139.

52 M. Cvek, M. Mrlik and V. Pavlinek, *J. Rheol.*, 2016, **60**, 687–694.

53 J. R. Morillas and J. de Vicente, *Soft Matter*, 2020, **16**, 9614–9642.

54 S. H. Piao, M. Bhaumik, A. Maity and H. J. Choi, *J. Mater. Chem. C*, 2015, **3**, 1861–1868.

55 F. Wang, Y. Ma, H. Zhang, J. Gu, J. Yin, X. Jia, H. Zhang, Y. Wang, X. Fu, R. Yu, Z. Wang, S. Han and G. Wang, *J. Mol. Liq.*, 2021, **324**, 115103.

56 D. S. Yoon, Y. J. Park and S. B. Choi, *Mech. Syst. Signal Process.*, 2019, **127**, 136–158.

57 Y. K. Wang, W. Y. Xie and D. F. Wu, *Carbohydr. Polym.*, 2020, **231**, 115776.

58 G. S. Wang, D. X. Zhao, N. N. Li, Y. Z. Zeng, S. Han, Y. Y. Ma, X. F. Dong and R. T. Yu, *J. Ind. Eng. Chem.*, 2019, **79**, 217–225.

59 H. B. Cheng, M. Wang, C. S. Liu and N. M. Wereley, *Smart Mater. Struct.*, 2018, **27**, 075030.

Footnotes

[†] Electronic supplementary information (ESI) available. See DOI: 10.1039/d1py00930c

Queries and Answers

Q1

Query: For your information: You can cite this article before you receive notification of the page numbers by using the following format: (authors), Polym. Chem., (year), DOI: 10.1039/d1py00930c.

Answer: Thank you for the information.

Q2

Query: Please confirm that the spelling and format of all author names is correct. Names will be indexed and cited as shown on the proof, so these must be correct. No late corrections can be made.

Answer: I hereby confirm that the spelling and format of all author names is correct.

Q3

Query: Do you wish to add an e-mail address for the corresponding author? If so, please provide the relevant information.

Answer: I wish to add 2 e-mail addresses for the correspondence:

cvek@utb.cz

jaroslav.mosnacek@savba.sk

Q4

Query: The first line of the Abstract has been inserted as the Graphical Abstract text; however, it currently exceeds the space available for the published version. Please check that the text is suitable and trim it so that it is shorter than 250 characters (including spaces).

Answer: Magnetic NPs grafted via mechano-ATRP served as a powerful agent for enhancing performance and stability of magnetorheological suspensions.